Int. J. Electrochem. Sci., 16 **(2021)** Article ID: 210763, doi: 10.20964/2021.07.06

International Journal of
ELECTROCHEMICAL
SCIENCE
www.electrochemsci.org

A Synergetic Effect Between Lithium Polysulfide Anchoring and Lithium Dendrite Suppression for High-performance Lithium-Sulfur Batteries Using Cellulose Paper

Ravindar Dharavath[1,*], *Ashwin Murali*[1], *T. S. Balasubramanian*[1], *and S. Gopinath*[1,2]

[1] Directorate of Power Supply Systems, Research Centre Imarat, Hyderabad 500069, Telangana, India
[2] Directorate of System Integration, Research Centre Imarat, Hyderabad 500069, Telangana, India
[*]E-mail: ravindar.d@rcilab.in

Received: 13 February 2021/ *Accepted:* 8 April 2021 / *Published:* 31 May 2021

This study aims to resolve the performance issues of Li–S batteries using KimWipes in three cell configurations cathode-side, anode-side, and both-sides. A no-KimWipe cell configuration is considered as a control. Substantial suppression of lithium polysulfide shuttling in the cathode-side configuration is observed owing to polar–polar interaction between higher-order dissolved polysulfides (Li_2S_8 to Li_2S_4) and abundant polar functional groups in the fibrous cellulose network of the KimWipes. On the anode side, KimWipes serve the dual roles of facilitating the homogeneous redistribution of Li ions during plating and stripping while minimizing the anchoring of polysulfide species migrating from the cathode. An electrochemical performance test is performed out at a C-rate of 0.1C, and the discharge-specific capacities at the first cycle for the cathode-side, anode-side, both-sides, and no-KimWipe cell configurations were 1,464.36, 1,286.95, 1,033.96, and 927.22 mAh g^{-1} S, respectively. Experimental testing is performed for upto 250 cycles for type II and III cells, which show good specific discharge, capacities as well as stable reversibility and coulombic efficiency. The cathode-side KimWipe cell configuration maintained stable reversibility with a higher coulombic efficiency. Results of this study will contribute towards realizing high-performance Li–S batteries for commercial applications.

Keywords: Li–S, anchoring, polar–polar interaction, KimWipe paper, lithium polysulfide

1. INTRODUCTION

Li–S batteries (LSBs) are advanced electrochemical systems with a theoretical specific capacity of 1,675 mAh g^{-1} S and a theoretical energy density of 2,600 Wh kg^{-1} both of which are high when compared with commercially available Li ion batteries [1]. Additionally, the S cathode is nontoxic, cost-effective, naturally abundant, and environmentally clean [2]; however, it also suffers from a polysulfide (PS)-shuttling effect, whereby the loss of active material from the cathode accelerates

capacity decay and low S utilization, whereby the density difference between S and lithium sulfide (Li_2S) reduces the performance of the cathode and ultimately destabilizes the cathode structure owing to volume expansion (~80%) [3, 4].

To address these issues, various strategies have been presented for improving the performance of S cathodes, such as introducing carbon host materials such as porous carbon [5], carbon nanotubes [6], carbon nanofibers [7], hierarchical carbon networks [8, 9], graphene [10], and graphene oxide [11]. However, although these carbon-host materials solve the problems of poor electrical conductivity and volume expansion during the charge–discharge process, they are inefficient at chemically anchoring the PS species [12] because the carbon-host material is nonpolar in nature whereas Li_2S_n is a polar material [13]. In contrast, this chemical anchoring can be improved through surface modification via polar heteroatom doping and codoping using O, N, S, P, B, and other elements [14–16].

Because of the importance of strong chemical interactions between a polar host material and polar PS, many studies have focused on exploring polar host materials, such as metal oxides, metal sulfides, and metal carbides, trapping PS species to achieve improved LSB performance [17-20]. Recently, polar materials have been synthesized and used in LSBs as multifunctional binders for suppressing the PS intermediate shuttle effect and reducing volume expansion owing to their elastic and mechanical properties [21, 22]. Similarly, polar additives have been rigorously investigated; e.g., nanoscale $Mg_{0.6}Ni_{0.4}O$, Al_2O_3, and La_2O_3 have been used in C–S cathodes to anchor the PS species and to improve their coulombic efficiency and cycling stability. However, polar oxide additives can anchor only small amounts of PS species owning to their low surface area and high density [23-25].

Apart from the problems with the S cathode, issues with the Li anode such as dendrite formation during the charge–discharge process and PS reduction on the metal surface also contribute significantly to lowering the electrochemical performance of the LSB, including its capacity retention and cycle life. Dendrite formation reduces the coulombic efficiency, safety, and Li utilization while increasing the polarization [3, 26, 27]. Various strategies have been suggested for suppressing dendrite formation with electrolyte additives such as HF, LiF, and $LiNO_3$ [28-30]. Of these, $LiNO_3$ is the most commonly used additive in LSBs however, the use of additives strengthens the solid electrolyte interphase layer of the Li anode. Continuous consumption of the additive impairs its effectiveness at suppressing dendrite growth over an increasing number of cycles [31]. Artificial protections such as tetraethoxysilane [32], Li nitride [33], composite coatings [34], and other surface coatings (e.g., Al_2O_3 [35], carbon [36], polymers, and alloys [37, 38]) have been introduced to stabilize the Li anode.

A new strategy has been reported for suppressing Li dendrites whereby a membrane comprising of polar functional groups is placed over the Li anode to inhibit the movement of Li ions toward protrusions and to achieve a smooth surface. Membranes such as 3D oxidized polyacrylonitrile (PAN) nanofiber layers and 3D glass-fiber cloth [39-41] facilitate an even distribution of Li ions and achieve a uniform and dendrite-free surface. Chang and co-workers used KimWipes as a membrane rich in polar functional groups to achieve a dendrite-free surface and improved reversibility for the Li foil. Fourier-transform infrared spectroscopy (FTIR) revealed the presence of abundant polar–OH groups and C–O–C chains in the fibrous cellulose network of a KimWipe. Li-plating tests were performed to assess the dendrite-inhibiting capability of the KimWipes; their results showed that Li plating occurred even at high current densities with delayed short-circuiting. They further reported that

KimWipes offer Li ion redistribution capability, mechanical stability, and excellent wettability. Compared with bare Li, the KimWipe-protected Li foil showed uniform Li deposition even after long operational times [42].

The present study is the first to evaluate the synergetic effect of using KimWipes in a coin cell with Li_2S_n anchoring on the cathode side and Li dendrite suppression on the anode side. Suppression of Li_2S_n shuttling occurs on the cathode side due to polar–polar interaction between the higher-order dissolved PS species (Li_2S_8 to Li_2S_4) and the abundant polar functional groups (C–O–C and –OH) present in the KimWipe. This abundance of chemically interactive polar functional groups, which can be used to successfully suppress Li dendrite formation and minimize the anchoring of PS from the S cathode that has migrated to the Li anode, is the principal motivation for using KimWipes. Fig. 1(a) shows the polar–polar interaction between the abundant polar functional groups (–OH and C–O–C) present in the cellulose membrane of a KimWipe and the multiple higher-order Li_2S_n species present in the S cathode. Fig. 1(b) shows the interaction between Li ions and polar functional groups, and Fig. 1(c) shows the interaction between PS species and KimWipes.

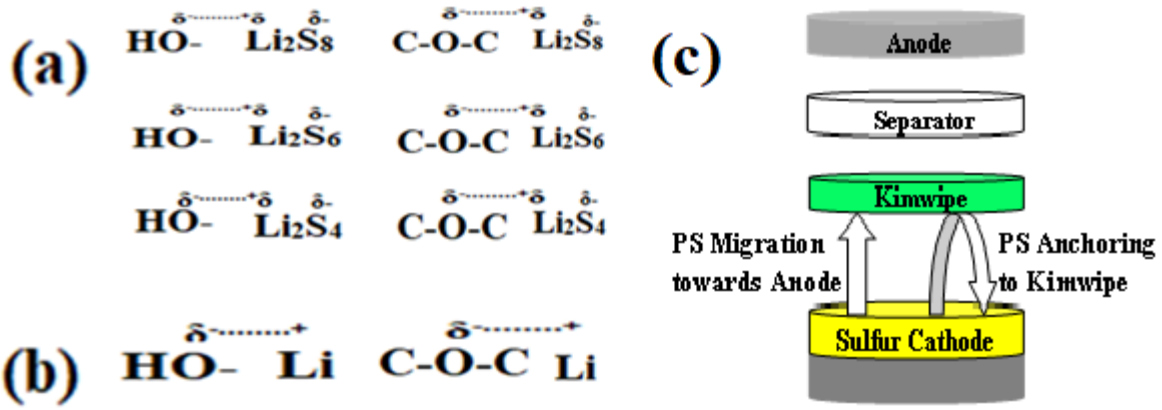

Figure 1. Schematics for (a) polar–polar interaction between the abundant polar functional groups in a KimWipe and the higher-order PS species on the cathode side; (b) polar–polar interaction between the abundant polar functional groups in the KimWipe and Li ions in the anode; and (c) interaction of PS species with the KimWipe.

2. EXPERIMENTAL

2.1 Material Preparation

Commercially available Li foil, elemental S, microporous carbon boiling chips, polyvinyledene difluoride (PVdF) binder, lithium bis (trifluoromethanesulfonyl) imide salt (LiTFSI), 1, 2-dimethoxyethane (DME), 1, 3-dioxolane (DOL), and tetraethylenglycol dimethoxyethane (TEGDME) were purchased from Sigma-Aldrich. All the materials have a purity of >99.99%. Carbon Black Super-P was purchased from Alfa Aesar and was used as received. KimWipes were purchased from Kimtech, and the Celgard 2500 separator was purchased from Celgard.

An electrolyte (DOL: DME: TEGDME with a volume ratio of 1:1:1) was prepared inside a standard four-port inert gas glove box (MBraun) by purging the high-purity Ar gas (99.9995%) to maintain a moisture and oxygen content of <1ppm. A cathode composite of microporous carbon and elemental S was subjected to thermal melt-diffusion inside a vacuum oven that was maintained at approximately 150°C–155°C for 6 h and then kept at 235°C for 2 h; this was done to ensure that any remaining superficial sulfur penetrated the pores of the carbon host. The cathode slurry was prepared by mixing the S–porous carbon composite, Carbon Black Super-P, and PVdF binder at a weight ratio of 80:10:10 in an N-methyl-2-pyrrolidone (NMP) solvent to form semiviscous slurry. The cathode composition was mixed for 2 h at 1,000 rpm to obtain homogeneous slurry, which was then coated onto an Al foil with a doctor blade and dried for 5 h to remove the NMP solvent and traces of moisture prior to integration into the coin cell.

2.2 Coin Cell Assembly Procedure

Four types of CR2025 cells were assembled inside a glovebox. Type I was assembled by sandwiching a Celgard 2500 separator between the Li-foil anode and the prepared cathode with no KimWipe. Type II was assembled by placing a KimWipe between the Li anode and the separator; this configuration was used to study dendrite suppression. Type III was assembled by placing the KimWipe between the separator and the cathode and was used to study PS anchoring. Finally, Type IV was prepared by placing one KimWipe between the separator and anode and another between the separator and the cathode; this configuration was used to analyze the synergetic effect of dendrite suppression and PS anchoring. Fig. 2 shows schematics of the cell configurations.

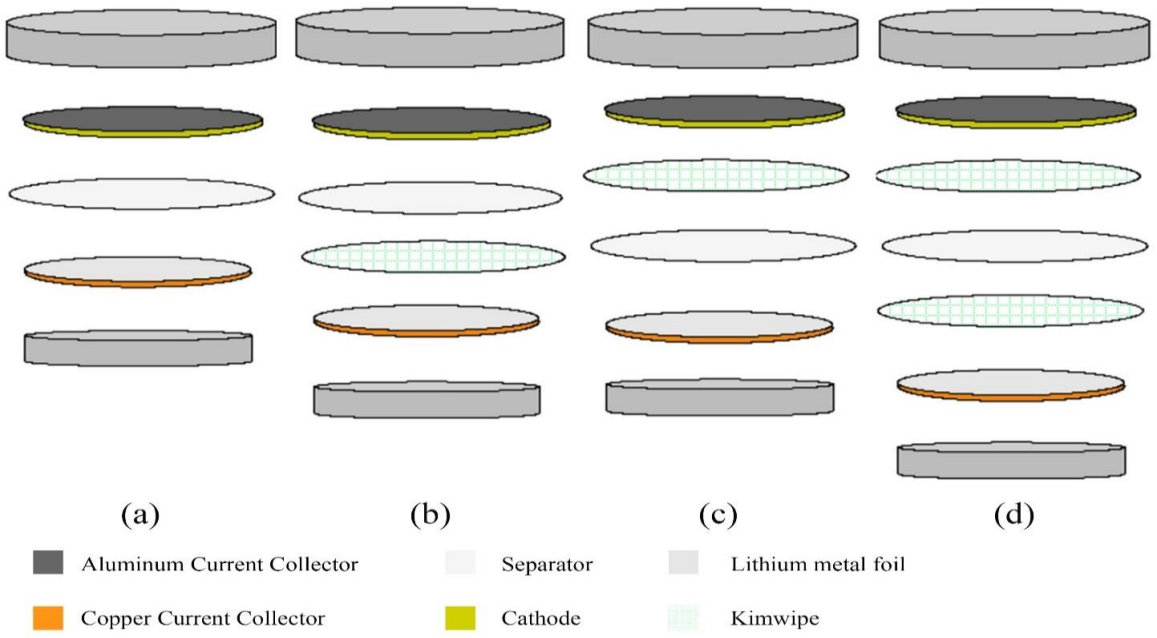

Figure 2. Schematic of the four types of cell configurations: (a) standard control cell without a KimWipe (type I), (b) KimWipe between the anode and Celgard separator (type II), (c) KimWipe between the cathode and Celgard separator (type III), and (d) KimWipe between the anode and the Celgard separator as well as between the cathode and Celgard separator (type IV).

2.3 Electrochemical Measurements

Electrochemical performance measurement was performed using the Biologic VSP-300 electrochemical workstation with a potential window between 1.4 and 2.6 V at a C-rate of 0.1C. A cyclic voltammeter was employed to study the oxidation and reduction peaks for the type I, II, III and IV cell configurations in the potential window of 1.0-3.0V at a scanning rate of $0.1mVs^{-1}$. An electrochemical impedance analysis was performed in the 200 kHz-100 mHz frequency region on a VSP-300 electrochemical workstation (BioLogic)

3. RESULT AND DISCUSSION

The electrochemical performance of various configurations of lithium-sulfur coin cells incorporating KimWipes was evaluated. Fig. 3(a) shows the charge–discharge curves at a C-rate of 0.1C for the first cycle. The specific capacities of types I–IV were 927.22, 1,286.95, 1,464.36, and 1,033 mAh g^{-1} S, respectively [43, 44].

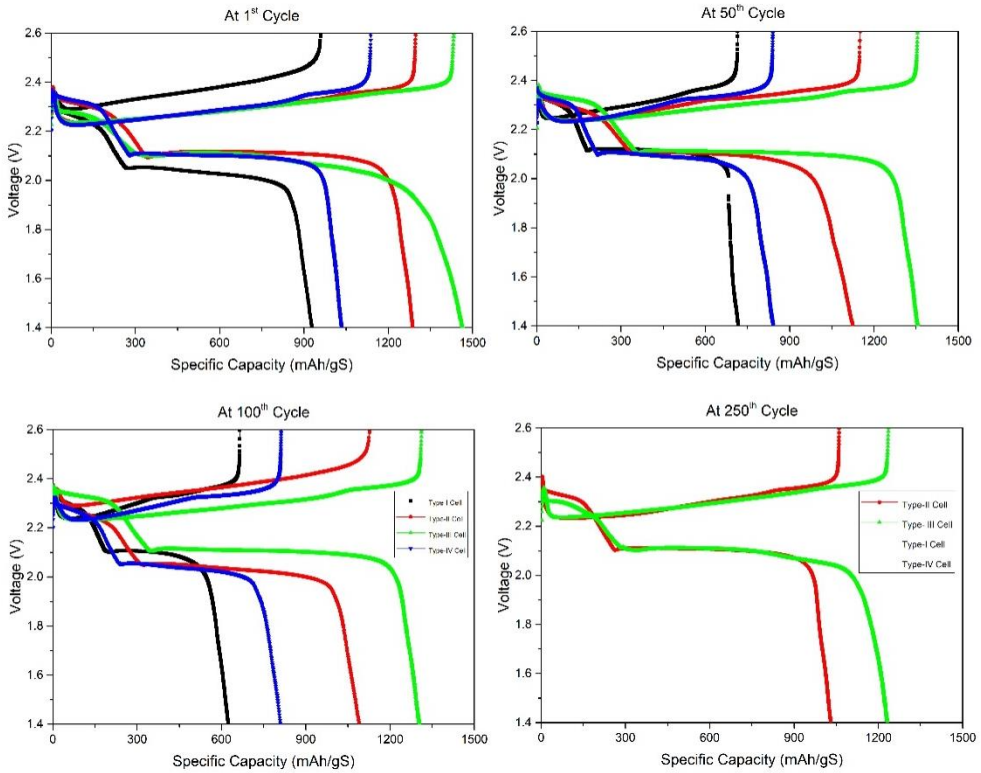

Figure 3. Charge–discharge curves for types I–IV at a C-rate of 0.1C in the voltage window of 1.4- 2.6 V under room temperature: (a) 1st cycle, (b) 50th cycle, (c) 100th cycle, and (d) 250th cycle.

Experimental data revealed that type I had a lower discharge specific capacity than types II–IV, this was attributed to the dissolution of soluble PS species into the electrolyte from the cathode side, leading to PS shuttling, loss of active material, and dendrite growth which in turn led to loss of lithium at the anode. Due to the potential difference, the dissolved PS tends to migrate toward the anode,

leading to a loss of active material on the anode side.

In type II, the KimWipe was placed between the anode and Celgard separator. The abundant polar functional groups present in the KimWipe had the dual functions of homogeneously redistributing Li ions by means of plating and de-plating on the anode surface and anchoring the dissolved PS species that migrated from the cathode, thereby improving the reversibility and coulombic efficiency.

In type III, the KimWipe was placed between the cathode and Celgard 2500 separator and exhibited a higher specific discharge capacity than the other cell configurations because of the KimWipe suppressed PS shuttling [45] on the cathode side. The improved electrochemical performance of the cell can be attributed to the polar interaction between the PS species on the S cathode and the abundant polar functional groups in the cellulose fibers of the KimWipe. The polysulfides on the S cathode were anchored by the polar functional groups of –OH and C–O–C in the KimWipe via weak polar interactions, which improved the specific capacity and resulted in good coulombic efficiency. The experimental data indicated a PS reduction and the anchoring of dissolved PS, which would otherwise migrate toward the anode and reduced its electrochemical performance.

In the type IV configuration KimWipes were placed between the Li anode and Celgard 2500 separator and between the cathode and Celgard 2500 separator. This configuration exhibited a lower discharge-specific capacity than type II and III though it was higher than that of type I cell. Placing KimWipes on both sides increased the electrochemical impedance owing to their insulating nature. This is clearly indicated by the voltage window for the type IV charge–discharge curve. The data for the 50^{th}, 100^{th}, and 250^{th} cycles are shown in Fig. 3(b-d), respectively, and reveals similar results. The type II and III cells maintained good electrochemical performance without any excessive capacity fading upto the 250^{th} cycle, whereas types I and IV exhibited appreciable capacity fading at the 100^{th} cycle. The abundant polar functional groups of the KimWipes provided dual functions: dendrite suppression on the Li anode side and anchoring of the PS species on the cathode side increasing in the No. of cycles [46].

A cyclic voltammetry (CV) study was performed for all four cell configurations, as shown in Fig. 4. The experimental data reveals that for the first scan of type I cell, two reduction peaks were observed at 2.15 and 1.65 V; these are attributed to the two-step reduction of elemental sulfur to lithium polysulfides. The peak at 2.15 V corresponds to the conversion of elemental sulfur to higher-order lithium polysulfides (Li_2S_n, $n \geq 4$); the next peak appeared at 1.65 V and was related to the formation of lower-order lithium polysulfides (Li_2S_n, $n \leq 4$). The anodic scan revealed only one oxidation peak at 2.70 V which can be attributed to conversion of lithium polysulfides into sulfur. The cathodic scanning of the type II cell revealed the same two reduction peaks at 2.17 and 1.79 V which are attributed to the conversion of sulfur to lithium polysulfides, and an anodic peak appeared at 2.73 V, indicating the conversion of lithium polysulfides to sulfur. Similarly types III and IV exhibited cathodic first peaks at 2.19 and 2.16 V and second peaks at 1.86 and 1.72 V, as well as anodic peaks at 2.67 and 2.72 V. The experimental results of CV revealed that the type III cell configuration has a high interface-reaction current which stimulates the conversion process, enhancing the cyclability. This can be seen in the cycling-discharge specific-capacity performance.

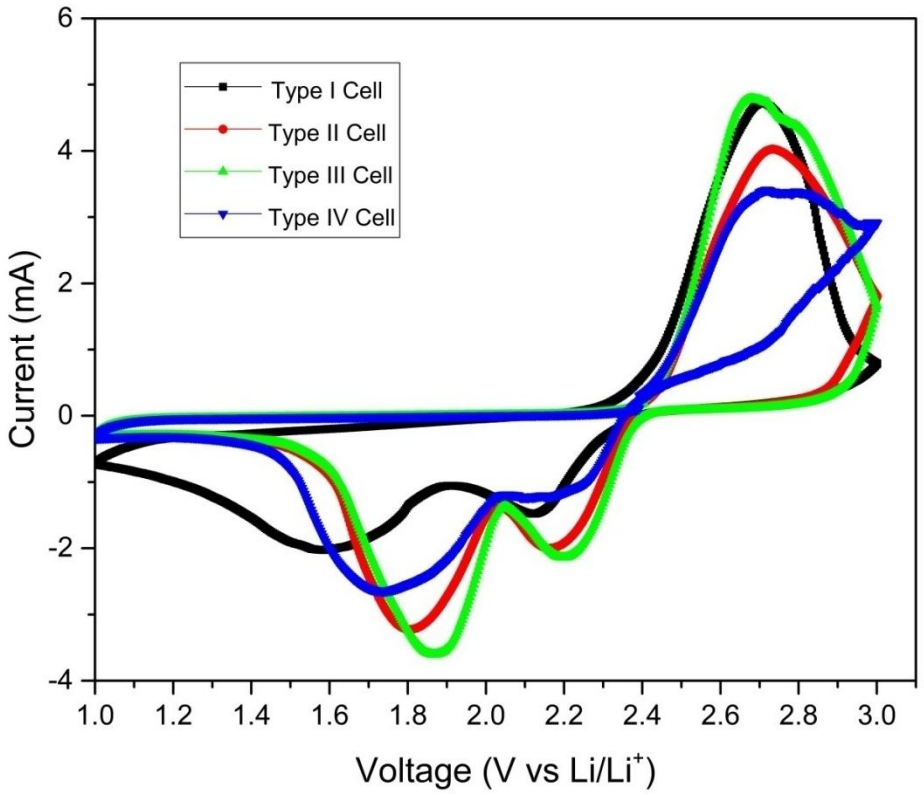

Figure 4. Comparison of the cyclic voltammograms for the type I–IV configurations with potential window from 1.0 to 3.0V at a scanning rate of 0.1mVs^{-1}

Electrochemical impedance analysis was performed in the 200 kHz-100 mHz frequency region on a VSP-300 electrochemical workstation (BioLogic). Type IV configuration had the highest electrochemical impedance, followed by types I, II, and III, as shown in Fig. 5. The type IV cell has two KimWipe interlayers (one each on anode and cathode sides) and exhibits a higher impedance subsequently, the discharge-specific capacity of the type IV cell is superior to that of the type I cell. The type III cell configuration has a lower electrochemical impedance and superior specific discharge capacity than the type I, II and IV cells. Types II and III have lower electrochemical impedance than type I, but exhibits similar results in terms of electrochemical performance.

Fig. 6 shows the discharge-specific capacity vs. the cycle number vs. the coulombic efficiency for all cell types. From the figure, it is apparent that, for the first few cycles, type I had a coulombic efficiency of >95%, which then decreased to <90% with the dissolution of PS species. However, the discharge-specific capacity remained >624.50 mAh g^{-1} S for all subsequent cycles upto the 100th cycle. Type II had a uniform coulombic efficiency of >95% due to the uniform plating and stripping of Li ions on the Li-anode surface and the anchoring of PS facilitated by the KimWipe and had a good discharge-capacity retention of 1,030.24 mAh g^{-1} S even upto 250 cycles.

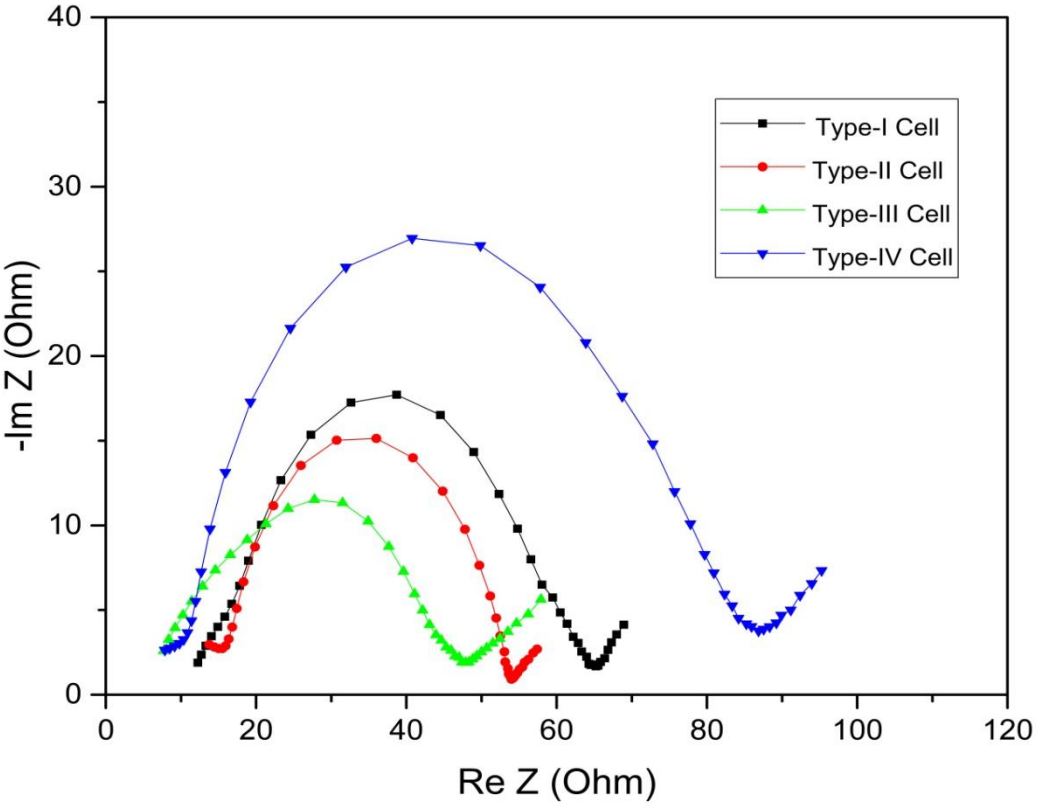

Figure 5. Comparison of the electrochemical impedances for type I–IV configuration at the frequency range of 200 kHz-100 mHz.

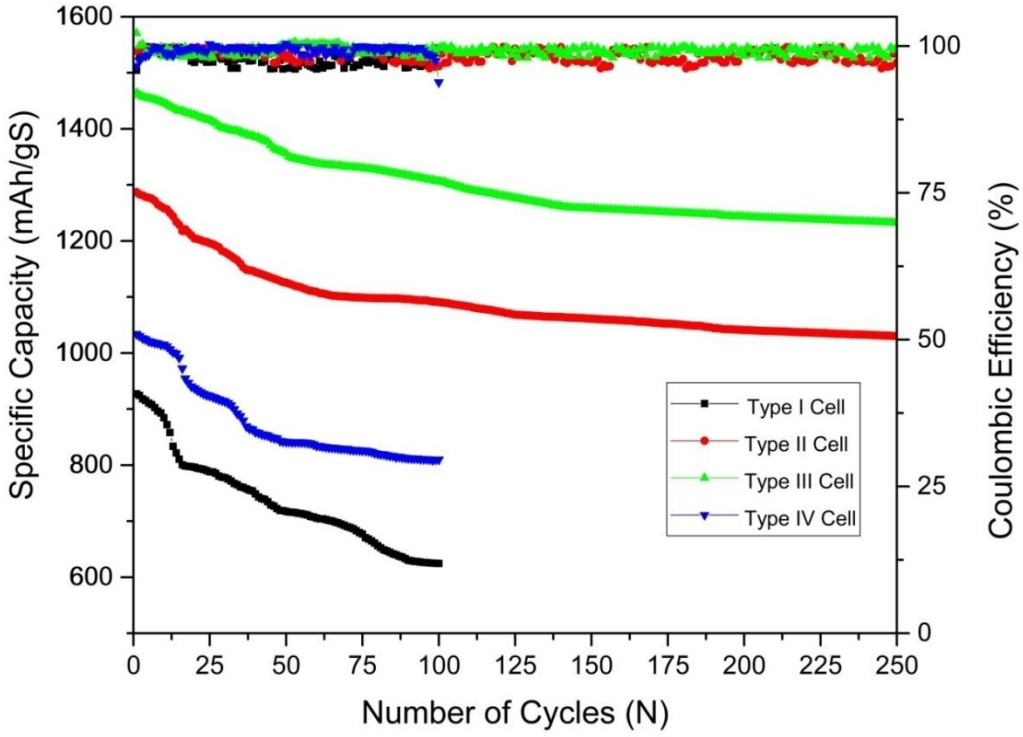

Figure 6. Discharge specific capacity vs. cycle number vs. coulombic efficiency for all types of cell configurations at a C-rate of 0.1C in a voltage window of 1.4 – 2.6 V under room temperature

The type III cell configuration exhibited a coulombic efficiency >95% which remained stable over a time. The type III cell maintained a good discharge-specific capacity of 1,232.07 mAh g^{-1} S at its 250th cycle; this was attributed to effective PS anchoring by polar functional groups in the cellulose membranes of the KimWipe, which minimized PS shuttling toward the anode. Type IV exhibit a good coulombic efficiency and discharge-specific capacity at the first cycle as well as comparatively good discharge-capacity retention 809.73 mAh g^{-1} S upto the 100th cycle.

4. CONCLUSION

Improvements in the electrochemical performance of LSBs using KimWipes were studied herein. The experimental results revealed that KimWipes have the synergistic effect of anchoring Li_2S_n at the cathode side while homogeneously redistributing Li ions on the anode side during plating and stripping. The type III (i.e., KimWipe on the cathode side) exhibited the highest specific capacity of 1,232.07 mAh g^{-1} S even upto the 250th cycle as well as the lowest electrochemical impedance; thus it has the best performance among all cell configurations. Our study demonstrates a cost-effective and facile approach for addressing the problems with LSBs and represents a step toward realizing their commercial applicability.

DATA AVAILABILITY
No data were used to support this study.

CONFLICTS OF INTEREST
The authors declare that there is no conflict of interest regarding the publication of this paper.

ACKNOWLEDGMENTS
The authors would like to acknowledge all the scientists of the Directorate of Power Supply Systems for their support and helpful discussions. This study was supported by the DRDO, The Ministry of Defence, Govt. of India project “Development of Li-S Rechargeable Batteries” (DLSRB) (Project No: ST/17-18/RCI-025).

References

1. S. Li, B. Jin, H. Li, C. Dong, B. Zhang, J. Xu, and Q. Jiang, *J. Electroanal. Chem*., 806 (2017) 41.
2. Z. Li, H. B. Wu, and X. W. David Lou, *Energy Environ. Sci*., 9 (2016) 3061.
3. J. Guo, and J. Liu, *Nanoscale Adv*., 1 (2019) 2104.
4. L. Yan, M. Xiao, S. Wang, D. Han, and Y. Meng, *J. Energy Chem*., 26 (2017) 522.
5. H. Gu, R. Zhang, P. Wang, S. Xie, C. Niu, and H. Wang, *J. Colloid Interface Sci*., 533 (2019) 445.
6. J. Wang, W. Wang, Y. Zhang, Y. Wang, and Y. Zhao, *Nanotechnology.*, 31 (2020) 025403.
7. Q. Li, J. Guo, J. Zhao, C. Wang, and F. Yan, *Nanoscale*., 11 (2019) 647.
8. Z. Zheng, H. Guo, F. Pei, X. Zhang, X. Chen, X. Fang, T. Wang, and N. Zheng, *Adv. Funct. Mater.*, 26 (2016) 8952.
9. R. Chen, T. Zhao, J. Lu, F. Wu, L. Li, J. Chen, G. Tan, Y. Ye, and K. Amine, *Nano Lett*., 13 (2013) 4642.

10. L. Duan, L. Zhao, H. Cong, X. Zhang, W. Lü, and C. Xue, *Small*., 15 (2019) 30663214.
11. G. Hu, C. Xu, Z. Sun, S. Wang, H. M. Cheng, F. Li, and W. Ren, *Adv. Mater*., 28 (2016) 1603.
12. Q. Zhang, Y. Wang, Z. W. Seh, Z. Fu, R. Zhang, and Y. Cui, *Nano Lett*., 15 (2015) 3780.
13. H. Wang, W. Zhang, J. Xu, and Z. Guo, *Adv. Funct. Mater*., 28 (2018) 1707520.
14. J. Cai, C. Wu, Y. Zhu, K. Zhang, and P. K. Shen, *J. Power Sources*., 341 (2017) 165.
15. C. P. Yang, Y. X. Yin, H. Ye, K. C. Jiang, J. Zhang, and Y. G. Guo, *ACS Appl. Mater. Interfaces.*, 6 (2014) 8789.
16. Q. Pang, J. Tang, H. Huang, X. Liang, C. Hart, K. C. Tam, and L. F. Nazar, *Adv. Mater*., 27 (2015) 6021.
17. T. Lei, Y. Xie, X. Wang, S. Miao, J. Xiong, and C. Yan, *Small*., 13 (2017) 1701013.
18. H. Wang, Q. Zhang, H. Yao, Z. Liang, H. W. Lee, P. C. Hsu, G. Zheng, and Y. Cui, *Nano Lett*., 14 (2014) 7138.
19. H. J. Peng, G. Zhang, X. Chen, Z. W. Zhang, W. T. Xu, J. Q. Huang, and Q. Zhang, *Angew. Chem. Int. Ed*., 55 (2016) 12990.
20. X. Liang, Y. Rangom, C. Y. Kwok, Q. Pang, and L. F. Nazar, *Adv. Mater*., 29 (2017) 1603040.
21. W. Chen, T. Qian, J. Xiong, N. Xu, X. Liu, J. Liu, J. Zhou, X. Shen, T. Yang, Y. Chen, and C. Yan, *Adv. Mater*., 29 (2017) 1605160.
22. H. Gao, Q. Lu, Y. Yao, X. Wang, and F. Wang, *Electrochim. Acta*., 232 (2017) 414.
23. M.-S. Song, S.-C. Han, H.-S. Kim, J.-H. Kim, K.-T. Kim, Y.-M. Kang, H.-J. Ahn, S. X. Dou, and J.-Y. Lee, *J. Electrochem. Soc*., 151 (2004) A791.
24. Y. J. Choi, B. S. Jung, D. J. Lee, J. H. Jeong, K. W. Kim, H. J. Ahn, K. K. Cho, and H. B. Gu, *Phys. Scr*., 2007 (2007) 62.
25. W. Zheng, X. G. Hu, and C. F. Zhang, *Electrochem. Solid-State Lett*., 9 (2006) A364.
26. C. P. Grey, and J. M. Tarascon, *Nat. Mater*., 16 (2016) 45.
27. H. Zhao, N. Deng, J. Yan, W. Kang, J. Ju, Y. Ruan, X. Wang, X. Zhuang, Q. Li, and B. Cheng, *Chem. Eng*. J., 347 (2018) 343.
28. S. Shiraishi, K. Kanamura, and Z.-i. Takehara, *J. Electrochem. Soc*., 146 (1999) 1633.
29. Y. Lu, Z. Tu, and L. A. Archer, *Nat. Mater*., 13 (2014) 961.
30. Jozwiuk, B. B. Berkes, T. Weiß, H. Sommer, J. Janek, and T. Brezesinski, *Energy Environ. Sci*., 9 (2016) 2603.
31. W. Li, H. Yao, K. Yan, G. Zheng, Z. Liang, Y. M. Chiang, and Y. Cui, *Nat. Commun*., 6 (2015) 7436.
32. G. A. Umeda, E. Menke, M. Richard, K. L. Stamm, F. Wudl, and B. Dunn, *J. Mater. Chem*., 21 (2011) 1593.
33. G. Ma, Z. Wen, M. Wu, C. Shen, Q. Wang, J. Jin, and X. Wu, *Chem. Commun*., 50 (2014) 14209.
34. C. Kozen, C. F. Lin, A. J. Pearse, M. A. Schroeder, X. Han, L. Hu, S. B. Lee, G. W. Rubloff, and M. Noked, *ACS Nano*., 9, (2015) 5884.
35. Z. Peng, S. Wang, J. Zhou, Y. Jin, Y. Liu, Y. Qin, C. Shen, W. Han, and D. Wang, *J. Mater. Chem. A.*, 4, (2016) 2427.
36. Y. J. Zhang, X. Y. Liu, W. Q. Bai, H. Tang, S. J. Shi, X. L. Wang, C. D. Gu, and J. P. Tu, *J. Power Sources*., 266 (2014) 43.
37. B. Zhu, Y. Jin, X. Hu, Q. Zheng, S. Zhang, Q. Wang, and J. Zhu, *Adv. Mater*., 29 (2017) 1603755.
38. X. Liang, Q. Pang, I. R. Kochetkov, M. S. Sempere, H. Huang, X. Sun, and L. F. Nazar, *Nat. Energy.*, 2 (2017) 17119.
39. Z. Liang, G. Zheng, C. Liu, N. Liu, W. Li, K. Yan, H. Yao, P. C. Hsu, S. Chu, and Y. Cui, *Nano Lett.*, 15 (2015) 2910.
40. X. B. Cheng, T. Z. Hou, R. Zhang, H. J. Peng, C. Z. Zhao, J. Q. Huang, and Q. Zhang, *Adv. Mater.*, 28 (2016) 2888.

41. B.-C. Yu, K. Park, J.-H. Jang, and J. B. Goodenough, *ACS Energy Lett*., 1 (2016) 633.
42. C.-H. Chang, S.-H. Chung, and A. Manthiram, *Adv. Sustainable. Syst*., 1 (2017) 1600034.
43. P. Rani, K. S. Kumar, A. D. Pathak, C. S. Sharma, *Appl. Surf. Sci*., 533 (2020) 147483.
44. D. Park, S. Park and D.-W. Kim, *Chem. Eng. J.*, 405 (2021) 126596.
45. X. Huang, Z. Wang, R. Knibbe, B. Luo, S. A. Ahad, D. Sun and L. Wang, *Energy Technol*., 7 (2019) 1801001.
46. Y.-C. Chien, R. Pan, M.-T. Lee, L. Nyholm, D. Brandell and M. J. Lacey, *J. Electrochem. Soc*., 166 (2019) A3235.